Available online at www.sciencedirect.com
SCIENCE DIRECT®
International Journal of Heat and Mass Transfer 48 (2005) 2841–2855
International Journal of HEAT and MASS TRANSFER
www.elsevier.com/locate/ijhmt

Influence of number of simulated particles on DSMC modeling of micro-scale Rayleigh–Bénard flows

Pei-Yuan Tzeng [a,*], Ming-Ho Liu [b]

[a] Department of Aeronautical Engineering, Chung Cheng Institute of Technology, National Defense University, Tahsi, Taoyuan 33509, Taiwan, ROC
[b] School of Defense Science, Chung Cheng Institute of Technology, National Defense University, Tahsi, Taoyuan 33509, Taiwan, ROC

Received 30 December 2004; received in revised form 31 January 2005

Abstract

Two-dimensional micro-scale Rayleigh–Bénard flows are investigated numerically using direct simulation Monte Carlo method. An enclosure of length-to-height aspect ratio of $AS = 4$ is taken to explore the influence of initial setting of simulated molecules. The simulation domain is divided into 81×21 sampling cells and the range of Rayleigh number from 3000 to 10000 corresponds to the convection state. Cases of 8, 10, 12, 14, 16 and 24 simulated particles in each collision cell are examined. It is shown that flow patterns with three-, four- or five-roll modes may appear depending on the number of simulated particles.

Keywords: Rayleigh–Bénard flow; DSMC; Convective flow pattern; Rarefied gas; Micro-scale flow

1. Introduction

Over the past few decades, the direct simulation Monte Carlo (DSMC) method has been the predominant predictive tool in rarefied gas flows. This approach was introduced by Bird [1] and has been applied to a variety of flow problems; for example, rarefied atmospheric gases, film growth and etching, and microsystems [2]. The DSMC method is a direct simulation method developed from kinetic theory. In this method, a large number of real gas molecules are modeled by a finite number of representative particles called simulated particles. The particle motions and the interparticle collisions are decoupled in a short time interval. Particle motions are modeled deterministically, whereas interparticle collisions are handled on a probabilistic basis in a small geometric cell called collision or computational cell or subcell. Macroscopic quantities are calculated by sampling particle properties in a particular cell called cell or sampling cell. Since the DSMC technique applies the cell network for the sampling of the macroscopic properties and for the selection of collision pairs, simulation results are good as long as the cell-size requirement on the macroscopic flow gradient resolution is satisfied and each of the cells contains sufficient simulated particles. It has been found that the collision cell size must be less than a mean free path [3,4] and each collision cell contains at least 5–10 [5] or 20 simulated particles [6].

* Corresponding author. Tel.: +886 3 390 8102; fax: +886 3 390 6419.
E-mail address: pytzeng@ccit.edu.tw (P.-Y. Tzeng).

0017-9310/$ - see front matter © 2005 Elsevier Ltd. All rights reserved.
doi:10.1016/j.ijheatmasstransfer.2005.01.017

Nomenclature

AS	aspect ratio L/H
d	molecular diameter [m]
Fr	Froude number v_h^2/gH
g	molecular gravity [m/s^2]
H	height of enclosure [m]
Kn	Knudsen number λ/H
k_B	Boltzmann constant
L	length of enclosure [m]
m	molecular weight [kg]
n	number density [1/m^3]
P	pressure [Pa]
Ra	Rayleigh number $(1024/125\pi)[(1-r_T)/(1+r_T)Kn]^2$
Ra_c	critical Rayleigh number
r_T	temperature ratio T_c/T_h
T	temperature [K]
U, V	dimensionless velocity components u/v_h, v/v_h
U^*, V^*	normalized velocity component $U/\lvert\vec{V}_{max}\rvert$, $V/\lvert\vec{V}_{max}\rvert$
$\vec{V}$	dimensionless velocity vector $\vec{V} = V\vec{i} + U\vec{j}$
u, v	dimensional velocity components [m/s]
v_h	most probable thermal speed $\sqrt{2k_BT_h/m}$ [m/s]
X, Y	dimensionless coordinates
x, y	Cartesian coordinates [m]

Greek symbols

θ	dimensionless temperature function $(T-T_c)/(T_h-T_c)$
λ	molecular mean free path [m]
ρ	density [kg/m^3]
τ	mean free time λ_0/v_h [s]

Subscripts

0	initial
c	cold wall
h	hot wall
R	right side of enclosure
L	left side of enclosure
M	middle of enclosure
max	maximum value

Superscripts

–	horizontal mean value
*	normalized value

The DSMC method has also been employed to simulate the vortices induced by thermally driven flow in temperature fields. The best known thermally driven flow is convective motions in a horizontal fluid layer heated from below, called Rayleigh–Bénard (RB) convection. In the RB convection, the convective vortex will appear when the temperature difference between the top and bottom fluid layers exceeds a critical value. The RB convection in continuum fluid dynamics have been widely studied in the past [7–11]. In recent years, many researchers have also directed attention to the RB convection in rarefied gases and a considerable number of numerical investigations using the DSMC method have been made.

Attempts to simulate the RB convection of a rarefied gas by the DSMC method were first reported by Garcia [12], who studied a rigid-free system with an aspect ratio of 1 at $Kn = 0.02$. Garcia and Penland [13] compared the DSMC results combined with principal oscillation pattern (POP) analysis with the numerical solution of linearized Navier–Stokes equations. Both approaches found that the results in DSMC simulation agreed closely with those obtained by the Navier–Stokes equations. Stefanov and Cercignani [14] employed the DSMC method to study the effects of various dimensionless control parameters on Bénard instability in a rarefied gas. Watanabe et al. [15] had shown that the determined critical Rayleigh number Ra_c of the RB system predicted by the DSMC method is in good agreement with that obtained by hydrodynamic equations. Golshtein and Elperin [16] investigated Bénard and thermal stress instabilities in a stratified rarefied gas with large temperature differences. The results illustrated that the DSMC method can be used to resolve the relatively slow vortex motion. Watanabe and Kaburaki [17] applied the DSMC method to simulate the transition of convection patterns in the three-dimensional RB system of length-to-width-to-height ratio 8:8:1 and 2:2:1 and discussed the effect of cell size on the onset of convection. The hexagonal roll patterns and the hysteresis in their transition were observed, and the onset of convection and the transition of convection patterns were affected by the sampling cell size. Hirano et al. [18] calculated the RB convection of the rarefied gas at $Ra = 2990$ under various Kn using the DSMC method and finite difference (FD) method. They found that the rarefaction effect causes the average temperature and the average vertical velocity in the rarefied gas to be higher than those in the continuum region. Stefanov et al. [19,20] compared the numerical solutions for RB convection of a rarefied monatomic gas by the DSMC method and by the FD method at a constant ratio of the cold and hot wall temperature under various Kn and Fr. The hysteresis loops between the co-existing attractors in the convection regime were also observed. All of these studies had supported that the DSMC method is a useful technique

for simulating the convection vortex formation in the rarefied gas. However, the influence of the number of simulated particles on the convective roll patterns in the RB system has rarely been examined in the past. This is important for the DSMC simulation of convective instabilities because the convective roll patterns are very sensitive to initial conditions.

In this paper, the convective vortex formation in the two-dimensional RB convection in a micro-scale enclosure is simulated using the DSMC method with various number of simulated particles and Ra in order to investigate the effects of the number of simulated particles on convective flow patterns under various Ra.

2. Problem statement

Consider a hard sphere of rarefied gas with molecular diameter $d = 3.7 \times 10^{-10}$ m and mass $m = 4.8 \times 10^{-26}$ kg in a horizontal two-dimensional rectangular enclosure of length L and height H as shown in Fig. 1. The aspect ratio ($AS = L/H$) of enclosure is chosen to be 4. In the present study, the calculation is performed under the same initial condition as that employed by Watanabe et al. [15]; namely, the initial temperature $T_0 = 80$ K and the initial pressure $P_0 = 20$ Pa, so that the number density is $n_0 = 1.81 \times 10^{22}$ m^{-3} and the mean free path is $\lambda_0 = 9.08 \times 10^{-5}$ m. The top wall temperature is $T_c = T_0$ and the bottom wall temperature is T_h. The gas is assumed to be heated from below, so that $T_h > T_c$. The acceleration of gravity g is chosen to be a hypothetical value, which is consistent with constant density, for the purpose of eliminating the density variations in the pure conduction state [12,13], i.e. $g = k_B(T_h - T_c)/mH$, where k_B is the Boltzmann constant. According to the Chapman–Enskog theory [21] for hard spheres, the Rayleigh number can be expressed as $Ra = (256/125\pi)[(T_h - T_c)/T_r Kn]^2$, where T_r is the reference temperature and defined as $T_r = (T_h + T_c)/2$, and Kn is the Knudsen number and defined as $Kn = \lambda_0/H$. In this simulation, we assume that initial molecular velocities are sampled from equilibrium Maxwellian distribution. Diffuse reflection boundary condition is imposed at the top and bottom walls, whereas specular reflection boundary condition is assumed at the boundaries on both sides.

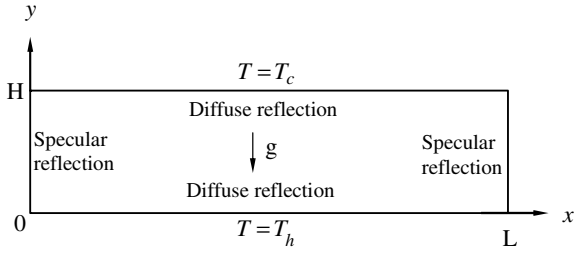

Fig. 1. Simulation region for the RB system.

3. Numerical method

In the present paper, we follow the DSMC algorithm [22] and investigate numerically the RB flow in a rarefied gas. The essence of the DSMC algorithm contains four important processes: move the molecules, index and cross-reference the molecules, simulate collisions, and sample the flow field. The molecular motions and intermolecular collisions are uncoupled over short-time intervals, and the collisions take place on a probabilistic basis. It is noted that the time interval should be less than the mean collision time and the collision cell size must be smaller than the mean free path. In the collision procedure, we follow the "No Time Counter (NTC)" scheme suggested by Bird [22] for the selection of collision pair. The Knudsen number Kn is set to be 0.01 and the range of Rayleigh number Ra is from 3000 to 10 000. The computational domain is divided into 81×21 sampling cells and 405×105 collision cells, so that each collision cell with linear dimension is smaller than local mean free path. To explore the influence of initial setting of simulated molecules, each collision cell initially contains 8, 10, 12, 14, 16 and 24 simulated particles on the calculation. They are denoted by Cases I–VI, respectively. The time step is 0.9 of mean collision time $\tau = \lambda_0/v_h$, where v_h is the most probable thermal speed $v_h = \sqrt{2k_B T_h/m}$, and a sampling is accomplished in every two simulated time steps.

4. Results and discussion

In this study, the stable convection flow patterns are our concern; therefore, we first examine how long the stable RB flow will achieve. Fig. 2 shows the time development of the mid-height ($Y = 1/2$) dimensionless temperatures near the left- and right-side boundaries (θ_L, θ_R) and at the middle of the simulation domain θ_M together with the horizontal average temperature $\bar{\theta}$ of Cases I and VI at $Ra = 3000$ and 10 000, respectively. The dimensionless temperature is defined as $\theta = (T - T_c)/(T_h - T_c)$. Here, the flow properties are averaged in every 100 times of sampling. As the figure indicates, the stable temperature fields can be observed after nearly 25 000 time steps. Since the number of simulated particles of Cases I and VI are the smallest and largest respectively, and the hot wall temperature and thermal velocity is the lowest at $Ra = 3000$ and the highest at $Ra = 10\,000$, one can safely deduce that the time steps where the convection flow patterns are stable may be less than 25 000 time steps for other simulation cases.

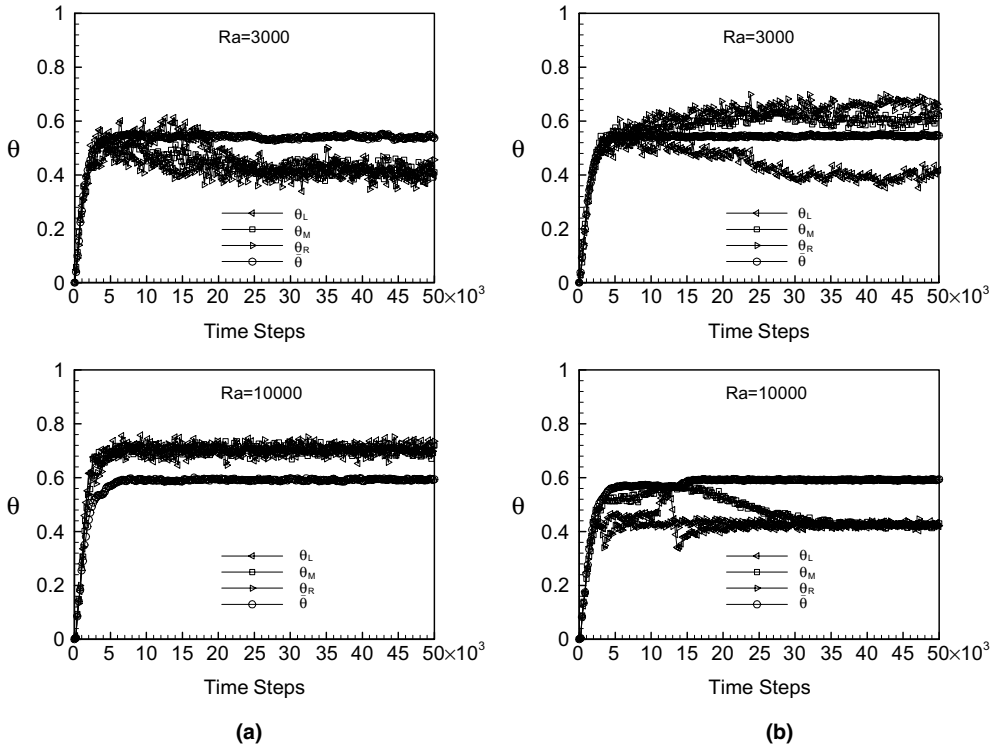

Fig. 2. The time-development of the mid-height temperature at $Ra = 3000$ and 10 000 for simulation Cases (a) I and (b) VI. (θ_L: left-side boundary, θ_R: right-side boundary, θ_M: in the middle of enclosure, $\bar{\theta}$: horizontal averaged.)

Actually, this assumption is valid in this study. According to the results, in the calculations, to insure that the RB flow is stable, sampling is started after 30 000 time steps and the flow properties are averaged over 20 000 time steps for each simulation case. According to this sampling method, for Case I, the fractional errors (or coefficient of variation) of temperatures at the middle of simulation domain and near the boundaries on both sides are approximately 5.31%, 5.78% and 6.82% at $Ra = 3000$ and 2.1%, 2.55% and 2.44% at $Ra = 10\,000$; for Case VI, they are nearly 2.46%, 4.28% and 2.77% at $Ra = 3000$ and 2.06%, 1.71% and 1.77% at $Ra = 10\,000$. The results illustrate that the fraction error becomes small for larger number of simulated particles and higher Ra.

Let us look closely at the changes in convective flow patterns of the flow fields for various Ra under constant number of simulated particles. The velocity vectors and isotherms at various Ra for Cases I–VI are shown in Figs. 3–8, respectively. In these figures, velocity vectors are normalized by the maximum velocity vector for each figure and defined as $\vec{V}^* = \vec{V} / |\vec{V}_{\max}|$. In Fig. 3 for Case I, in which each collision cell initially contains eight simulated particles, the flow patterns are five-roll modes at $Ra = 5000$, 8000 and 9000 and four-roll modes at the others. One may notice that the appearance of the four- or five-mode is uncertain as Ra increases in this case. In addition, it is worth noting that the rotational flow directions of convection rolls are not always identical for the same number of rolls at some Ra. For example, the flow patterns at $Ra = 3000$, 4000, 6000, 7000 and 10 000 are all four-roll modes; the arrangement of convection rolls from the left- to right-side boundaries is $(-,+,-,+)$ at $Ra = 3000$, 4000 and 6000, but it is $(+,-,+,-)$ at $Ra = 7000$ and 10 000, where the $-$ and $+$ are the symbol for the counterclockwise- and clockwise-rotating vortex flows, respectively. From a mathematical point of view, the four-roll structure of $(-,+,-,+)$ and that of $(+,-,+,-)$ are two different solutions; however, from a physical point of view, they are all the same solutions. Since the side walls are assumed to be specular reflection boundary conditions, the RB convective flow possesses periodic structures in the x-direction. Accordingly, the counterclockwise- and clockwise-rotating vortex flows in the RB convection are equivalent. The reversed rotational flow directions are probably due to the small numerical disturbances in the DSMC computations.

Fig. 4 shows Case II, in which there are 10 simulated particles per collision cell initially. As the figure indicates, the flow pattern is a five-roll mode of $(-,+,-,+,-)$ at $Ra = 4000$, a four-roll mode of $(+,-,+,-)$ at $Ra = 7000$ and four-roll modes of $(-,+,-,+)$ at the

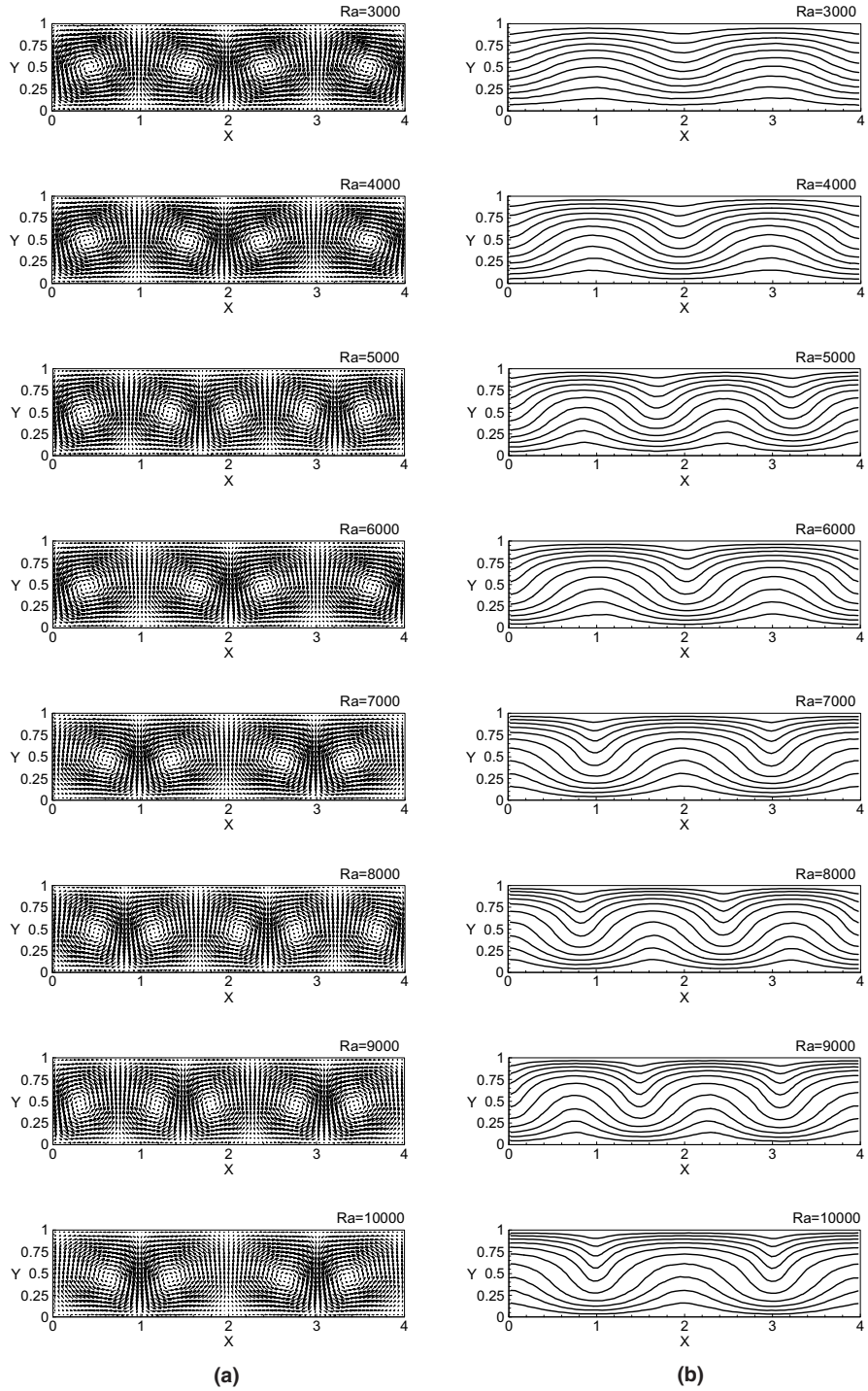

Fig. 3. The velocity vectors and isotherms at various *Ra* for Case I. (a) Velocity vectors and (b) isotherms.

rest of *Ra*. The results show that the flow patterns are comparatively consistent and the effects of the changes in *Ra* on the flow patterns are very small for this case. For a larger number of simulated particles, 12 simulated particles per collision cell (Case III) in Fig. 5, the development of flow pattern is not consistent as *Ra* increases. The flow patterns are four-roll modes at $Ra = 3000$, 4000 and turn to five-roll modes at

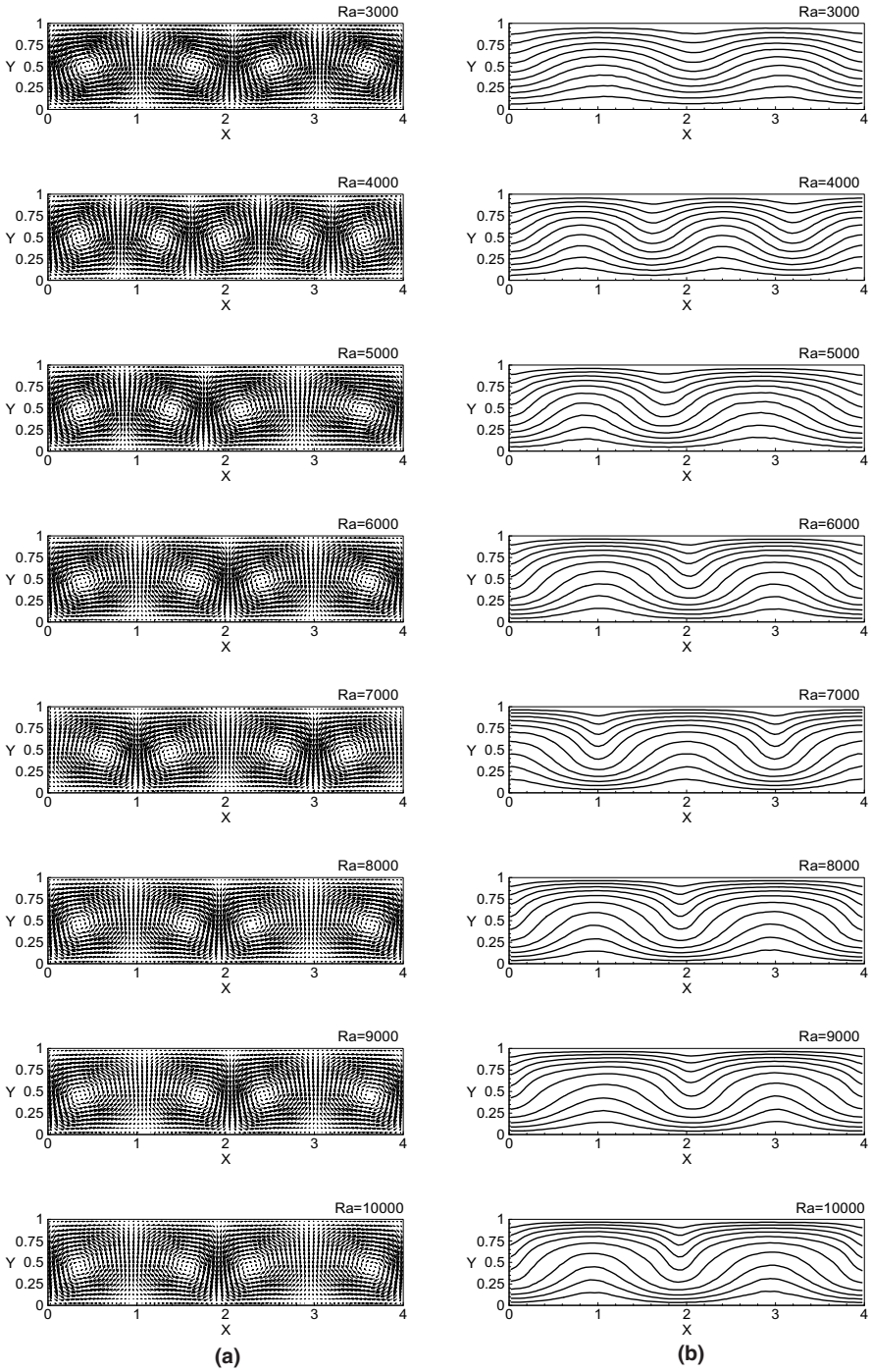

Fig. 4. The velocity vectors and isotherss at various *Ra* for Case II. (a) Velocity vectors and (b) isotherms.

Ra = 5000, 6000; however, it alternates between a four- and five-roll mode as *Ra* increases from 7000 to 10 000. It can be seen from the results that for Case III, the probability of appearance of four-roll mode is equal to that of five-roll mode.

For Case IV in Fig. 6, each collision cell contains 14 simulated particles initially, there are respective flow patterns in two different ranges of *Ra*. At *Ra* = 3000–7000, the flow patterns are four-roll modes, but at *Ra* = 8000–10 000, they are five-roll modes. Though the

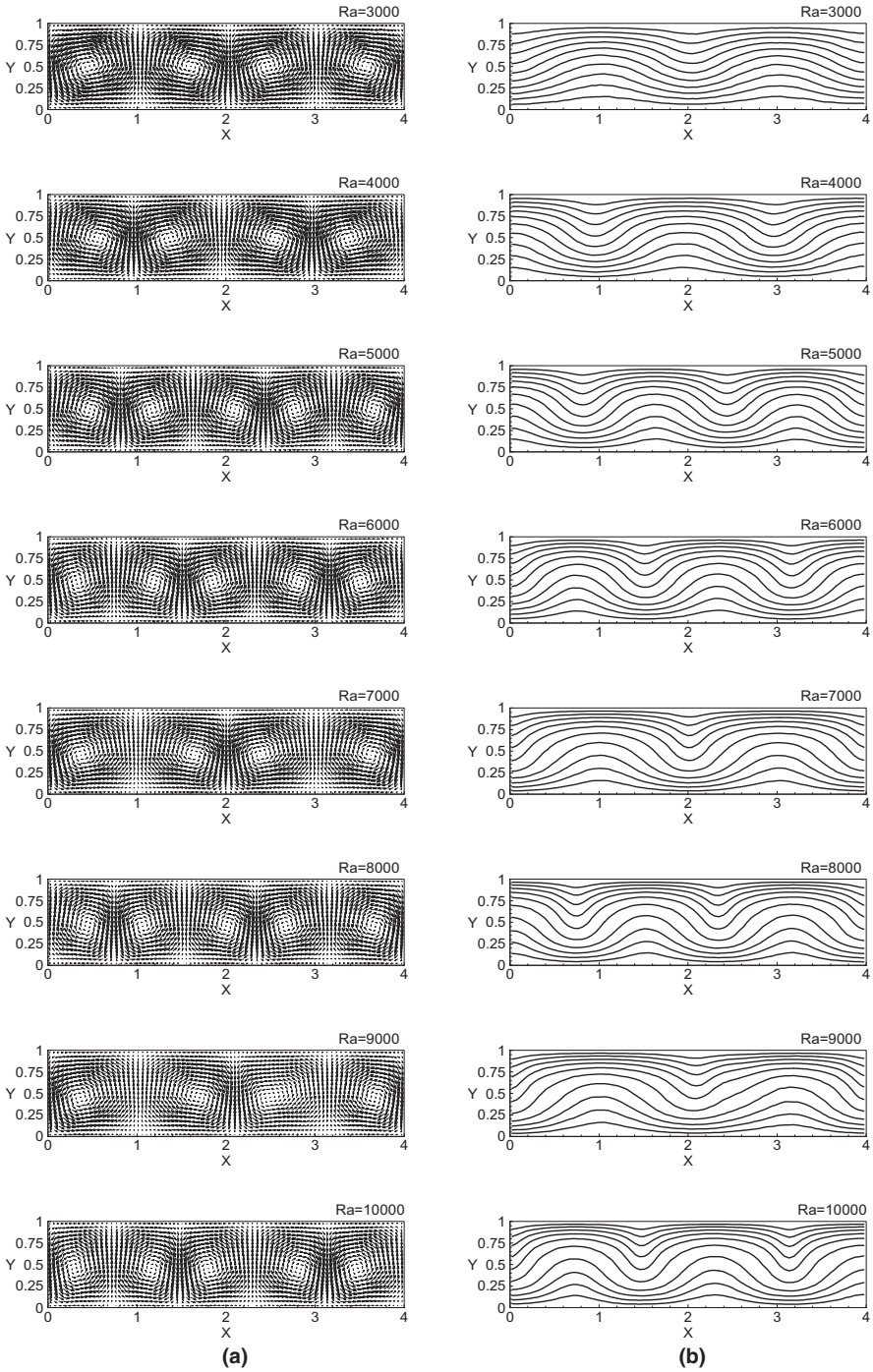

Fig. 5. The velocity vectors and isotherms at various *Ra* for Case III. (a) Velocity vectors and (b) isotherms.

flow mode changes at higher *Ra*, the flow patterns are consistent at these two ranges of *Ra*. As the initial setting of number of simulated particles per collision cell increases to 16, for Case V in Fig. 7, the flow patterns are five-roll modes of $(+,-,+,-,+)$ at $Ra = 3000$, 6000 and 9000 and four-roll modes of $(-,+,-,+)$ at other *Ra*. It is obvious that the flow pattern alternates between a five-roll mode and two four-roll modes as *Ra* increases from 3000 to 10000. Furthermore, when the flow fields at various *Ra* have the same number of convective rolls,

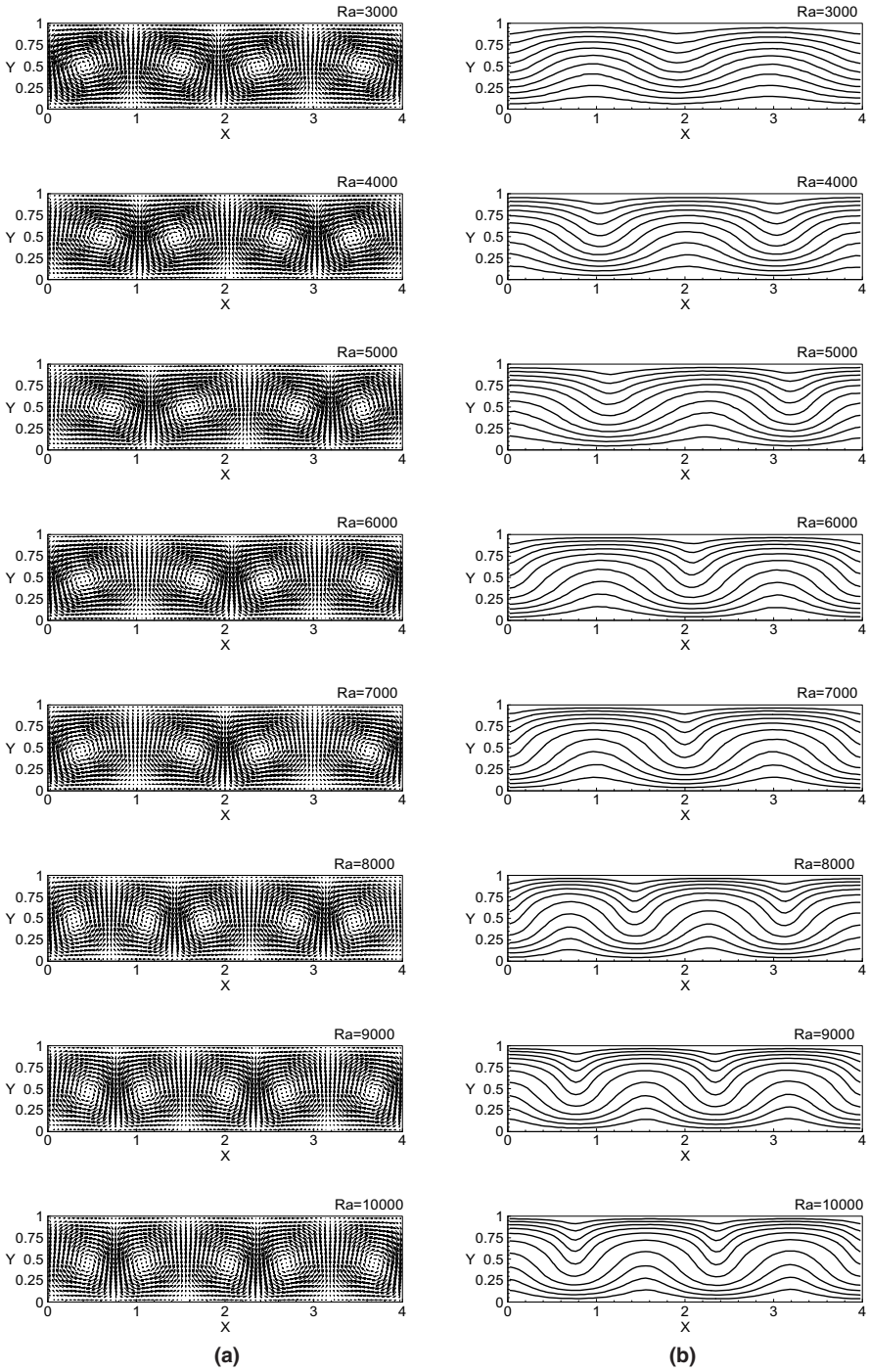

Fig. 6. The velocity vectors and isotherms at various *Ra* for Case IV. (a) Velocity vectors and (b) isotherms.

the arrangements of their vortices flow directions are identical. Accordingly, we may say that the change of flow pattern with increasing *Ra* is more regular in this case.

For Case VI, the initial setting of simulated particles in each collision cell increases further to 24, the flow patterns are not always four- or five-roll modes, as shown in Fig. 8. They are three-roll modes of $(-,+,-)$ at

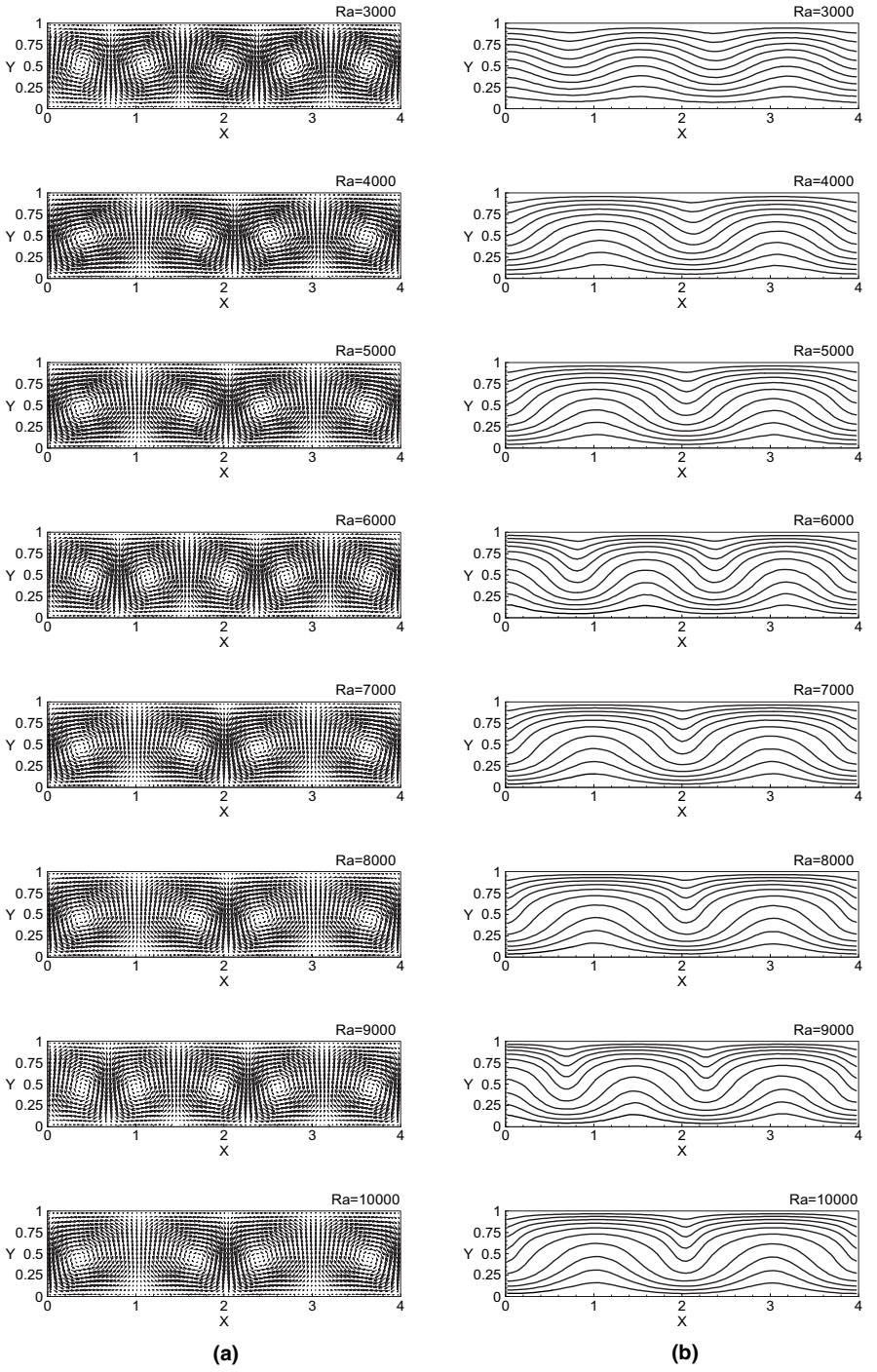

Fig. 7. The velocity vectors and isotherms at various *Ra* for Case V. (a) Velocity vectors and (b) isotherms.

Ra = 3000, four-roll modes of $(-,+,-,+)$ at *Ra* = 5000, 8000 and 10000 and $(+,-,+,-)$ at *Ra* = 9000, and five-roll modes of $(-,+,-,+,-)$ at *Ra* = 6000 and 7000 and $(+,-,+,-,+)$ at *Ra* = 4000. It is clear that the larger number of simulated particles may still result in the change in flow pattern which becomes irregular as *Ra* increases. Moreover, it must be noted that the flow pattern is not a four- or five-roll mode but a three-roll mode at

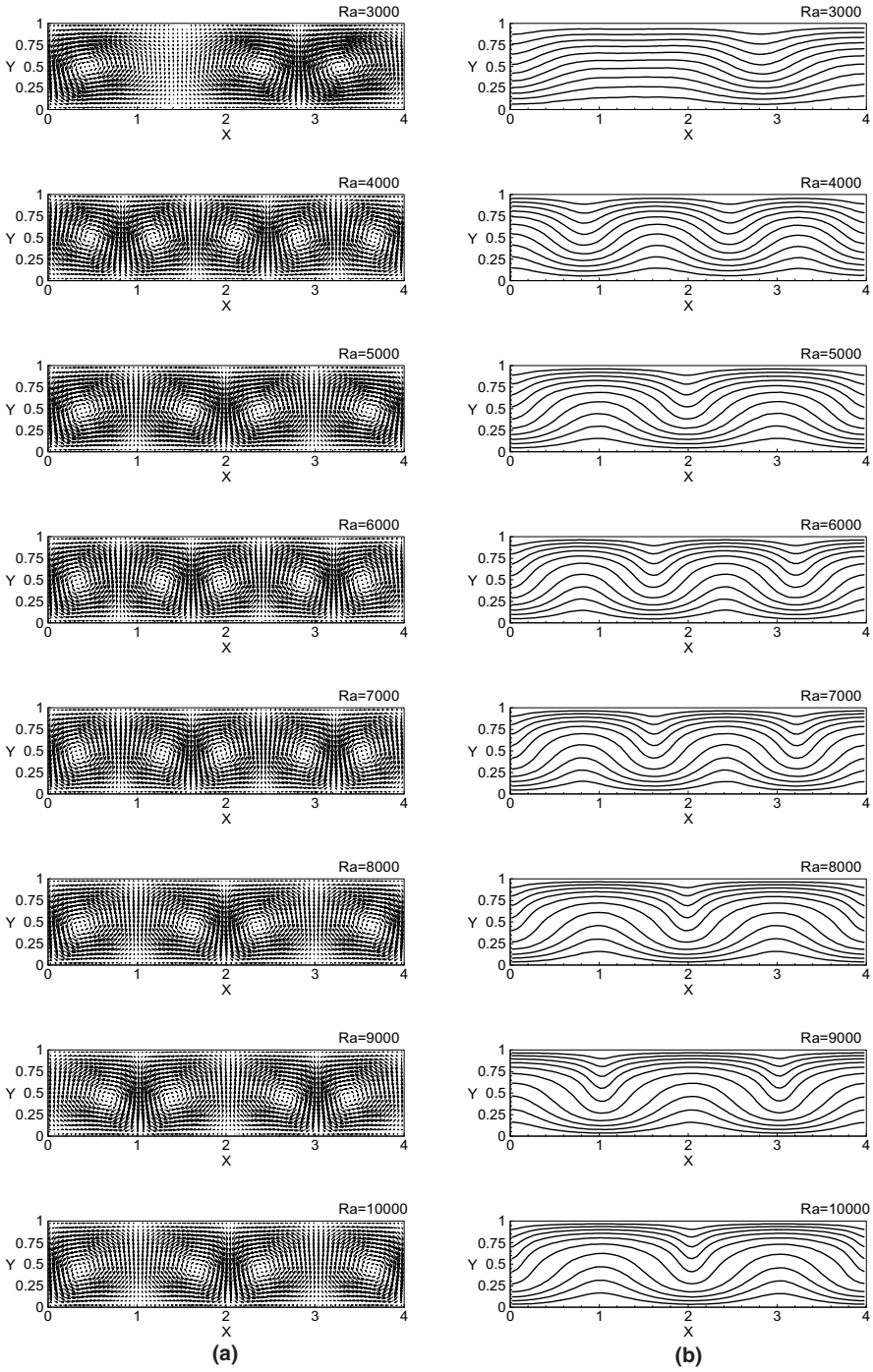

Fig. 8. The velocity vectors and isotherms at various *Ra* for Case VI. (a) Velocity vectors and (b) isotherms.

Ra = 3000 for this case. In Fig. 8, the isotherms between *X* = 1 and 2 are almost parallel to the bottom/top walls at *Ra* = 3000. In other words, the temperature gradients in the horizontal direction are almost zero; therefore, convective rolls can not develop in this region, and the flow pattern in the enclosure is a three-roll mode.

We can see from these figures the change in convective flow patterns at constant *Kn* under various *Ra*

calculated by the DSMC method with different number of simulated particles. One may notice that the flow patterns are either four- or five-roll modes in these simulations, except that it is a three-roll mode at $Ra = 3000$ for Case VI. However, in the continuum regime, the numerical solutions obtained by the Navier–Stokes equations with horizontal enclosure of $AS = 4$ are always four-roll modes [23]. In other words, in some cases, the convection flow structures are not in compliance with the hydrodynamic solutions. Other DSMC simulations [14,16] had also found similar results that flow structure was a two- or three-roll mode for $AS = 2$. It can be attributed to the influence of rarefaction, the error induced by the specular reflection boundary conditions or the numerical fluctuation induced by the simulated particles chosen in the DSMC simulation. In addition, it might be caused by the increase in initial hot wall temperature induced by increasing Ra at constant Kn, because the RB flow is very sensitive to the initial conditions. There is one further result that we must not ignore. In this simulation, the changes in flow patterns are always among three- to five-roll modes. This is the effect of the enclosure of length-to-height aspect ratio chosen as $AS = 4$. The results show that the stability of the solutions for Cases II and IV are superior to the others. As can be seen, the flow patterns in Case II are always four-roll modes except for $Ra = 4000$, and those in Case IV are all four-roll modes at $Ra \leqslant 7000$ and five-roll modes at $Ra \geqslant 8000$, respectively. We therefore conclude that the simulation with larger number of simulated particles can not yield stable solutions in RB convection.

We now concentrate on the changes in flow patterns at constant Ra under various numbers of simulated particles. Table 1 summarizes the convective flow patterns for various Ra under different numbers of simulated particles. For $Ra = 3000$, the flow patterns are four-roll modes for Cases I –IV, five-roll mode for Case V and three-roll mode for Case VI. This indicates that the increase in number of simulated particles can cause the number of rolls to increase or decrease under constant initial conditions. As Ra increases to 4000 and 5000, two five-roll modes for Cases II and VI for the former and Cases I and III for the latter can be observed, and four-roll modes occur for the other cases. It is clear that the probability of the occurrence of four- and five-roll modes for $Ra = 4000$ is equal to that for $Ra = 5000$. For a higher Rayleigh number, $Ra = 6000$, they are four-roll modes for Cases I, II and IV and five-roll modes for Cases III, V and VI. It is obvious that the number of occurrences of four-roll mode is the same as that of five-roll mode at $Ra = 6000$. At $Ra = 7000$, the flow patterns are four-roll modes for all cases except a five-roll mode for Case VI. This demonstrates that the influence of the number of simulated particles on the formation of convective flow pattern is small. At $Ra = 8000$ and 9000, the flow patterns for Cases II, V and VI are four-roll modes and those for Cases I, III and IV are five-roll modes at $Ra = 8000$, and four-roll modes are for Cases II, III and VI and five-roll modes are for the rest of cases at $Ra = 9000$. The probability of occurrence of the four-roll mode is equal to that of the five-roll mode for these two Rayleigh numbers. As Ra further increases to 10000, the flow patterns are four-roll modes for Cases I, II, V and VI and five-roll modes for Cases III and IV. It is clear that the number of cases of four-roll mode is again more than that of five-roll mode.

As seen from the results of this simulation, the flow pattern can be influenced by the different initial setting

Table 1
The convective flow patterns at various Ra for different simulation cases

Ra		3000	4000	5000	6000	7000	8000	9000	10000
Convective flow pattern	Case I	4 −+−+	4 −+−+	5 −+−+−	4 −+−+	4 +−+−	5 +−+−+	5 −+−+−	4 +−+−
	Case II	4 −+−+	5 −+−+−	4 −+−+	4 −+−+	4 +−+−	4 −+−+	4 −+−+	4 −+−+
	Case III	4 −+−+	4 +−+−	5 +−+−+	5 −+−+−	4 −+−+	5 +−+−+	4 −+−+	5 −+−+−
	Case IV	4 −+−+	4 +−+−	4 +−+−	4 −+−+	4 −+−+	5 −+−+−	5 +−+−+	5 +−+−+
	Case V	5 +−+−+	4 −+−+	4 −+−+	5 +−+−+	4 −+−+	4 −+−+	5 +−+−+	4 −+−+
	Case VI	3 −+−	5 +−+−+	4 −+−+	5 −+−+−	5 −+−+−	4 −+−+	4 +−+−	4 −+−+

of number of simulated particles under the same initial conditions in the RB convection flow and the dual or triple solutions may occur. This might be due to the thermodynamically unequivalent initial conditions at microscopic level induced by the various initial setting of number of simulated particles. Since the DSMC method is a probabilistic simulation method and it uses simulated particles that move and collide in physical space to accomplish a direct simulation of the molecular gas dynamics. The selection of collision pair employs the NTC scheme and intermolecular collisions are treated on a probabilistic rule. Macroscopic flow properties are obtained by sampling particle properties in a sampling cell. When the simulations use different number of simulated particles, the selected collision pairs and their post-collision properties may vary. Accordingly, the same initial conditions from the macroscopic point of view might be different from that from the microscopic point of view. The RB convection flow is very sensitive to the disturbances. The changes in microscopic properties induced by the different initial setting number of simulated particles in the DSMC computations might yield a preferred one of the three possible flow patterns which are three-, four- and five-roll modes. However, the possibility of formation of three-roll modes is the lowest. It is interesting to note that the probability of the occurrence of five-roll modes increases as Ra increases to 9000 except for $Ra = 7000$, and then it decreases at $Ra = 10\,000$ again. This may be caused by the increase in thermal fluctuations induced by increasing Ra.

The preceding discussion is from the qualitative point of view. Let us turn to the variations in flow properties among the different simulation cases at constant Ra from the quantitative point of view. In this simulation, there are four types of flow patterns for various Ra: one three-, one five- and four four-roll modes for $Ra = 3000$, four four- and two five-roll modes for $Ra = 4000$, 5000 and 10 000, three four- and three five-roll modes for $Ra = 6000$, 8000 and 9000, and five four- and one five-roll modes for $Ra = 7000$. Accordingly, the cases for $Ra = 3000$, 4000, 6000, 7000 are chosen for illustration.

Fig. 9(a)–(d) show the dimensionless temperature θ and vertical velocity component V profiles at the center of enclosure ($X = 2$) for various cases at $Ra = 3000$, 4000, 6000, 7000, respectively. In Fig. 9(a) for $Ra = 3000$, for Cases I– IV, the slopes of θ decrease as Y increases and vertical velocity V are all negative, and there is just a little variation in θ and V among these cases. The result shows that the flow patterns for these cases are the same and their flow properties in quantitative terms are very close. For Case V, the slope of θ decreases as the height increases from bottom wall to middle height, then it increases as the height increases from middle height to top wall; moreover, velocity V at all heights are almost zero. This indicates that the flow direction in the upper region is opposite to that in the lower region; therefore, a convective roll is formed in the middle of enclosure and its center is at the center of enclosure, as shown in Fig. 7. The distributions of θ and V for Case VI are different from those for the above cases. Accordingly, the flow pattern for Case VI is not the four- or five-roll mode but the three-roll mode.

In Fig. 9(b) for $Ra = 4000$, for Cases I and V, the slopes of θ decrease and vertical velocity V are all negative; however, for Cases III and IV, the slopes of θ increase and vertical velocity V are all positive. This indicates that the flows in the middle region of enclosure go downward for Cases I and V, but they go upward for Cases III and IV. Accordingly, the flow patterns for Cases I and V and Cases III and IV are four-roll modes of $(-,+,-,+)$ and $(+,-,+,-)$, respectively, as shown in Figs. 3, 5, 6 and 7. It is worth noting that the values of θ and V for Cases I and V are very close and those for Cases III and IV are almost equal. This demonstrates that the macroscopic flow properties remain almost unchanged quantitatively for the same flow patterns which are obtained by simulation under constant initial conditions with different number of simulated particles. For Cases II and VI, the slopes of θ decrease as Y increases from 0 to 0.5, then they increase as Y increases from 0.5 to 1. It is clear that the shapes of the curve of θ for Cases II and VI are different from those for the other cases. Therefore, the flow patterns are five-roll modes, as shown in Figs. 4 and 8. It must be noted that the vertical velocity V at all levels of Y for Case II is a little positive and velocity V for Case VI is higher than that for Case II; therefore, the center of the vortex in the middle region of enclosure is close to $X = 2$ for Case II and deviates from $X = 2$ for Case VI.

Fig. 9(c) shows the profiles of θ and V at $X = 2$ for various cases at $Ra = 6000$. As the figure indicates, they are considerably close for Cases I, II and IV. Since the flow patterns for these three cases are all four-roll modes of $(-,+,-,+)$ as shown in Figs. 3, 4 and 6, the result also shows that the macroscopic flow properties are steady and independent of the initial setting of number of simulated particles for the same flow patterns. For Cases III, V and VI, the shape of curves of θ and V are similar, whereas the flow patterns are five-roll modes of $(-,+,-,+,-)$ for Cases III and VI shown in Figs. 5 and 8 and $(+,-,+,-,-)$ for Case V shown in Fig. 7. However, it can be seen from Fig. 9(c) the deviations in θ and V between Cases III and VI are larger than those between Cases V and VI. The flow direction of the vortex in the center region of flow field for Case V is opposite to that for Cases III and VI, but the center of them are around $X = 2$; therefore, the shape of curve of θ and V for these three cases are similar. However, the center of the vortex in the center region of enclosure for Cases V and VI are closer to $X = 2$ than for Case III. Therefore, the vertical velocity V for Cases V and VI

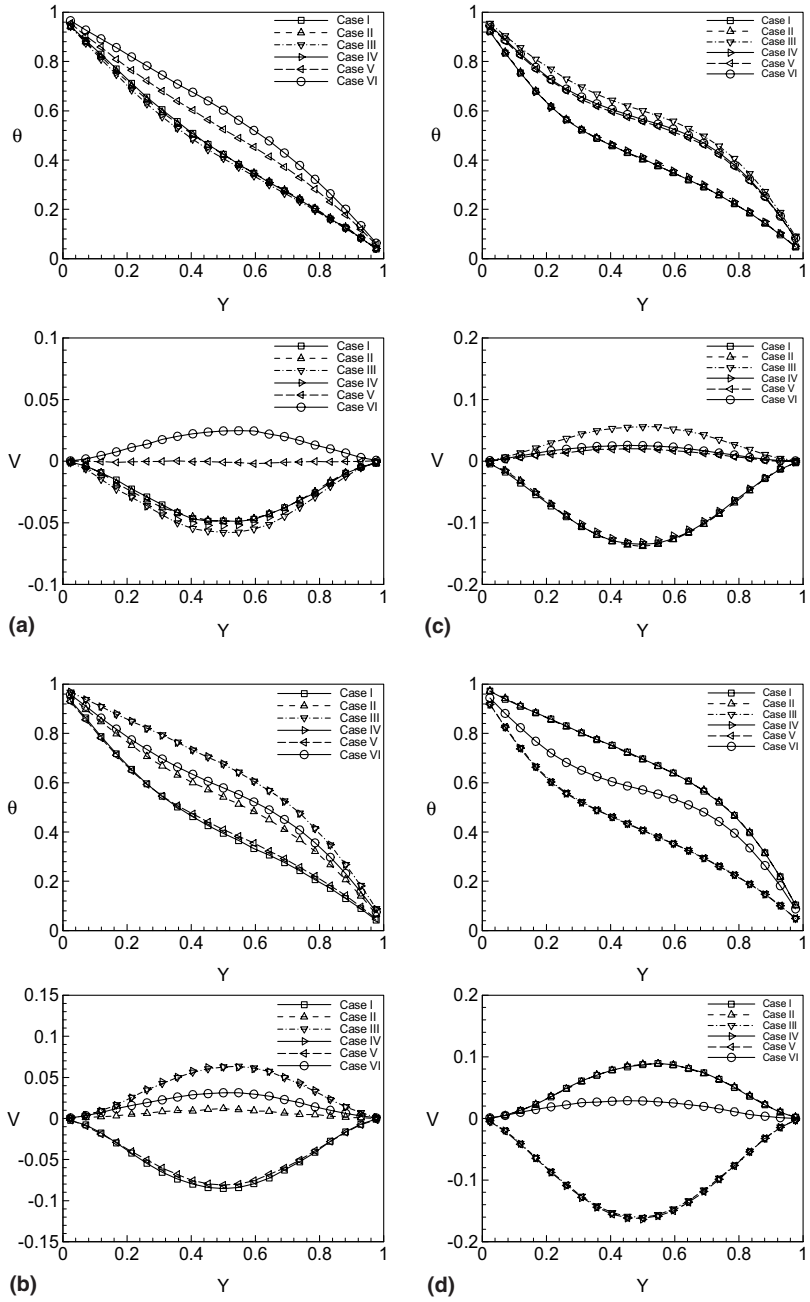

Fig. 9. Dimensionless temperature θ and vertical velocity V profiles at $X = 2$ for various simulation cases at $Ra = 3000$, 4000, 6000, and 7000. (a) $Ra = 3000$, (b) $Ra = 4000$, (c) $Ra = 6000$ and (d) $Ra = 7000$.

are closer to 0 than for Case III, and their deviations are smaller than those between Cases III and VI. At $Ra = 7000$ in Fig. 9(d), the θ and V at all heights of Y for Cases I and II are almost completely equal, while those for Cases III, IV and V are also nearly equivalent. In addition, the slopes of curves of θ and V for Cases I and II are opposite to those for Cases III, IV and V. Accordingly, the number of convection rolls are equal for all cases but the flow directions of vortices for the former two cases are reverse to those for the latter three cases. As Figs. 3–7 indicate, at $Ra = 7000$, the flow patterns are four-roll modes of $(+,-,+,-)$ for Cases I and II and $(-,+,-,+)$ for the other cases. The result illustrates that the macroscopic flow properties are also

unchanged for the same flow patterns in both cases. It is worth noting that the distributions of θ and V for Case VI are different from those for Cases I –V. The shapes of curves of θ and V for Case VI are similar to those for Case VI at $Ra = 6000$; therefore, its flow pattern is a five-roll mode of $(-,+,-,+,-)$ as shown in Fig. 8.

From the results mentioned above, if the flow patterns obtained by simulation under constant initial conditions with different numbers of particles have the same number of rolls and flow directions, their flow properties are almost constant. In other words, they are slightly influenced by the number of particles. In addition, the quantitative consistency for four-roll mode is better than that for five-roll mode and the deviations of flow properties among different cases for high Ra are smaller than those for low Ra. This shows that the influence of the number of simulated particles on the flow structure of five-roll mode and high Ra is stronger than that of four-roll mode and low Ra in this study. Since the fraction errors of flow properties for low Ra are larger than those for high Ra, the deviations of flow properties are larger for low Ra. The flow pattern in the x-direction is assumed to possess the periodic structure, but the flow near the boundary on each side might not form a complete convection roll, for example, 2/3 and 1/3 of roll are formed near the right- and left-side boundaries respectively. However, both side boundaries are in specular reflection conditions, that is to say, the temperature should be symmetric to the side boundary and there is no temperature gradient in the x-direction at the side boundary. Accordingly, the convective roll must be symmetric to the side boundary. This causes imperfect convective roll near the boundary on each side intending to form a perfect roll and the flow pattern is a five-roll mode in the enclosure of $AS = 4$. Since the simulation with different initial setting of number of simulated particles might cause the flow near side boundaries to develop convective rolls in different size, the size of inner convection rolls in the enclosure might also be changed. Accordingly, the flow properties obtained by calculating with the different number of simulated particles might be varied at the same position in the flow field. For the four-roll mode, the number of rolls is the same as the aspect ratio of enclosure of $AS = 4$, the size of each roll is almost equal; therefore, the number of simulated particles has very little influence on the flow properties.

5. Conclusions

A numerical investigation for a two-dimensional micro-scale RB flow has been performed by the DSMC method with different initial setting of number of simulated particles. It was found that the flow patterns in the RB convection are three-, four- and five-roll structures for an enclosure of $AS = 4$, and the number of convection rolls and their rotational flow directions can be influenced by the different number of simulated particles and Rayleigh number. In this simulation, the solutions obtained by the DSMC method using a larger number of simulated particles are not more stable than those using less particles as Ra increases. In addition, it shows that the macroscopic flow properties obtained by the different cases under constant initial conditions remain unchanged for the same number of rolls and the same flow directions. Our results suggest that a suitable number of simulated particles can decrease the influence of numerical fluctuation on the flow patterns, and it is necessary when simulating RB convection which is sensitive to the disturbances.

Acknowledgement

The study was partially supported by the National Science Council of Taiwan, the Republic of China through Grant No. NSC-93-2212-E-014-004.

References

[1] G.A. Bird, Approach to translational equilibrium in a rigid sphere gas, Phys. Fluids 6 (1963) 1518–1519.
[2] E.S. Oran, C.K. Oh, B.Z. Cybyk, Direct simulation Monte Carlo: recent advances and applications, Ann. Rev. Fluid Mech. 30 (1998) 403–441.
[3] G.A. Bird, Direct simulation of the incompressible Kramers problem, Prog. Astronaut. Aeronaut. 51 (1977) 323–333.
[4] J.N. Moss, G.A. Bird, Direct simulation of transitional flow for hypersonic re-entry conditions, Prog. Astronaut. Aeronaut. 96 (1985) 113–139.
[5] G.A. Bird, The direct simulation Monte Carlo method: current status and perspectives, in: M. Mareschal (Ed.), Microscopic Simulations of Complex Flows, Plenum, New York, 1990, pp. 1–13.
[6] F.J. Alexander, A.L. Garcia, B.J. Alder, Cell size dependence of transport coefficients in stochastic particle algorithms, Phys. Fluids 10 (6) (1998) 1540–1542.
[7] S. Chandrasekhr, Hydrodynamic and Hydromagnetic Stability, Clarendon Press, Oxford, NY, 1961, pp. 9–75.
[8] K.-T. Yang, Transitions and bifurcations in laminar buoyant flows in confined enclosures, ASME J. Heat Transfer 110 (1988) 1191–1203.
[9] E. Koschmieder, Bénard Cells and Taylor Vortices, Part I, Cambridge University Press, Cambridge, England, UK, 1993.
[10] A.V. Gelting, Rayleigh–Bénard Convection: Structures and Dynamics, World Scientific, Singapore, 1998.
[11] E. Bodenschatz, W. Pesch, G. Ahlers, Recent developments in Rayleigh–Bénard convection, Ann. Rev. Fluid Mech. 32 (2000) 709–778.
[12] A.L. Garcia, Hydrodynamic fluctuations and the direct simulation Monte Carlo method, in: M. Mareschal (Ed.),

Microscopic Simulations of Complex Flows, Plenum, New York, pp. 141–162.
[13] A.L. Garcia, C. Penland, Fluctuating hydrodynamics and principal oscillation pattern analysis, J. Stat. Phys. 64 (5/6) (1991) 1121–1132.
[14] S. Stefanov, C. Cercignani, Monte Carlo simulation of Bénard's instability in a rarefied gas, European J. Mech. B/Fluids 11 (5) (1992) 543–553.
[15] T. Watanabe, H. Kaburaki, M. Yokokawa, Simulation of a two-dimensional Rayleigh–Bénard system using the direct simulation Monte Carlo method, Phys. Rev. E 49 (5) (1994) 4060–4064.
[16] E. Golshtein, T. Elperin, Convective instabilities in rarefied gases by direct simulation Monte Carlo method, J. Thermophys. Heat Transfer 10 (2) (1996) 250–256.
[17] T. Watanabe, H. Kaburaki, Particle simulation of three-dimensional convection patterns in a Rayleigh–Bénard system, Phys. Rev. E 56 (1) (1997) 1218–1221.
[18] H. Hirano, M. Seo, H. Ozoe, Two-dimensional numerical computation for Rayleigh–Bénard convection with both the Navier–Stokes equation and the Boltzmann equation, Model. Simulat. Mater. Sci. Eng. 10 (2002) 765–780.
[19] S. Stefanov, V. Roussinov, C. Cercignani, Rayleigh–Bénard flow of a rarefied gas and its attractors. I. Convection regime, Phys. Fluids 14 (7) (2002) 2255–2269.
[20] S. Stefanov, V. Roussinov, C. Cercignani, Rayleigh–Bénard flow of a rarefied gas and its attractors. II. Chaotic and periodic convection regime, Phys. Fluids 14 (7) (2002) 2270–2288.
[21] S. Chapman, T.G. Cowling, The Mathematical Theory of Non-uniform Gases, third ed., Cambridge University Press, Londan, 1970, p. 168.
[22] G.A. Bird, Molecular Gas Dynamics and Direct Simulation of Gas Flow, Clarendon Press, Oxford, NY, 1994, Chapter 11.
[23] C.-Y. Soong, P.-Y. Tzeng, D.-C. Chiang, T.-S. Sheu, Numerical study on mode-transition of natural convection in differentially heated inclined enclosures, Int. J. Heat Mass Transfer 39 (14) (1996) 2869–2882.